

Graded index separate confinement heterostructure transistor laser: analysis of various confinement structures

Mohammad Hosseini¹, Hassan Kaatuzian^{1,*}, and Iman Taghavi²

¹Photonics Research Laboratory, Electrical Engineering Department, Amirkabir University of Technology, Tehran 15914, Iran

²Electrical and Computer Engineering Department, Georgia Institute of Technology, Atlanta, GA, 30332, USA

*Corresponding author: hsnkato@aut.ac.ir

Received October 31, 2016; accepted February 24, 2017; posted online March 21, 2017

A new configuration of the confinement structure is utilized to improve optoelectronic performance, including threshold current, ac current gain, optical bandwidth, and optical output power of a single quantum well transistor laser. Considering the drift component in addition to the diffusion term in electron current density, a new continuity equation is developed to analyze the proposed structures. Physical parameters, including electron mobility, recombination lifetime, optical confinement factor, electron capture time, and photon lifetime, are calculated for new structures. Based on solving the continuity equation in separate confinement heterostructures, the threshold current reduces 67%, the optical output power increases 37%, and the -3 dB optical bandwidth increases to 21 GHz (compared to 19.5 GHz in the original structure) when the graded index layers of $\text{Al}_\xi\text{Ga}_{1-\xi}\text{As}$ ($\xi:0.05 \rightarrow 0$ in the left side of quantum well, $\xi:0 \rightarrow 0.02$ in the right side of quantum well) are used instead of uniform GaAs in the base region.

OCIS codes: 250.5960, 140.0140, 230.0230, 250.0250, 270.0270.
doi: 10.3788/COL201715.062501.

Carrier transport across the separate confinement heterostructure (SCH) has substantial effects on dc and ac characteristics of quantum well (QW) lasers^[1]. Also, the carrier population of QW excited states, which depends on the confinement structure, plays an important role in the threshold specifications of SCH and graded index (GRIN) SCH QW lasers^[2]. The heterojunction bipolar transistor laser (HBTL) is a type of QW laser, containing one (or a few) QW(s) and two SCHs in its base region, where the carrier dynamics are governed by various structural factors. The transistor laser (TL) that we study here is based on an npn heterojunction bipolar transistor (HBT) (n-InGaP/p-GaAs/n-GaAs) with an emitter area of $4000 \mu\text{m}^2$ ^[3]. In GaAs-based HBTs, the common approach to establish a quasi-electric field is linearly grading the aluminum (or indium) content of AlGaAs (or InGaAs)^[4]. In this Letter, we employ GRIN layers of $\text{Al}_\xi\text{Ga}_{1-\xi}\text{As}$ instead of simply uniform GaAs in the base region to achieve various levels of confinement.

The energy band diagram of the primary TL proposed by Feng and Holonyak^[3] under forward bias is depicted in Fig. 1(a), named the first structure in this Letter. In the first proposed design, called the second structure, the GRIN layers of $\text{Al}_\xi\text{Ga}_{1-\xi}\text{As}$ ($\xi:0.05 \rightarrow 0$ in SCH1, $\xi:0 \rightarrow 0.02$ in SCH2) are used [Fig. 1(b)]. In the third structure, GRIN layers of $\text{Al}_\xi\text{Ga}_{1-\xi}\text{As}$ ($\xi:0.07 \rightarrow 0.02$ in SCH1, $\xi:0.02 \rightarrow 0$ in SCH2) are used [Fig. 1(c)]. Calculating the slope of the conduction band profile, we gain an estimate for the induced built-in potential in SCH1 and SCH2. The energy gap of the $\text{Al}_\xi\text{Ga}_{1-\xi}\text{As}$ material (in eV) at $\xi < 0.45$ is determined by $E_g(\text{Al}_\xi\text{Ga}_{1-\xi}\text{As}) =$

$1.424 + 1.247\xi$. The induced built-in potential can be achieved using $\varepsilon = \Delta E_g/qW_{\text{SCH}}$, where W_{SCH} is the SCH width, and ΔE_g denotes the bandgap energy difference at two sides of the SCH regions, resulting in a magnitude of ~ 11 and ~ 12 kV/cm for the induced built-in potential of SCH1 and SCH2, respectively. These values of quasi-electric fields are in good agreement with the experimental values reported in Refs. [4,5].

To analyze the proposed structures, the equation for the electron current density, including both drift and diffusion components, can be written as

$$J_n = qD_n \left(\frac{qn\varepsilon}{kT} + \frac{\partial n}{\partial x} \right), \quad (1)$$

where n is the base electron concentration, and D is the diffusion constant. The continuity equation describing the injected minority electron population transporting from the emitter to the collector is

$$\frac{\partial n}{\partial t} = \frac{1}{q} \frac{\partial J_n}{\partial x} - \frac{n}{\tau_B}, \quad (2)$$

where τ_B is the base recombination lifetime. Combining Eqs. (1) and (2), the following equations for the SCH1 and SCH2 regions can be obtained under the steady-state condition ($\partial n/\partial t = 0$):

$$D_1 \frac{\partial^2 n}{\partial x^2} + \mu_1 \varepsilon_1 \frac{\partial n}{\partial x} - \frac{n}{\tau_{B1}} = 0 \quad \text{SCH1}, \quad (3)$$

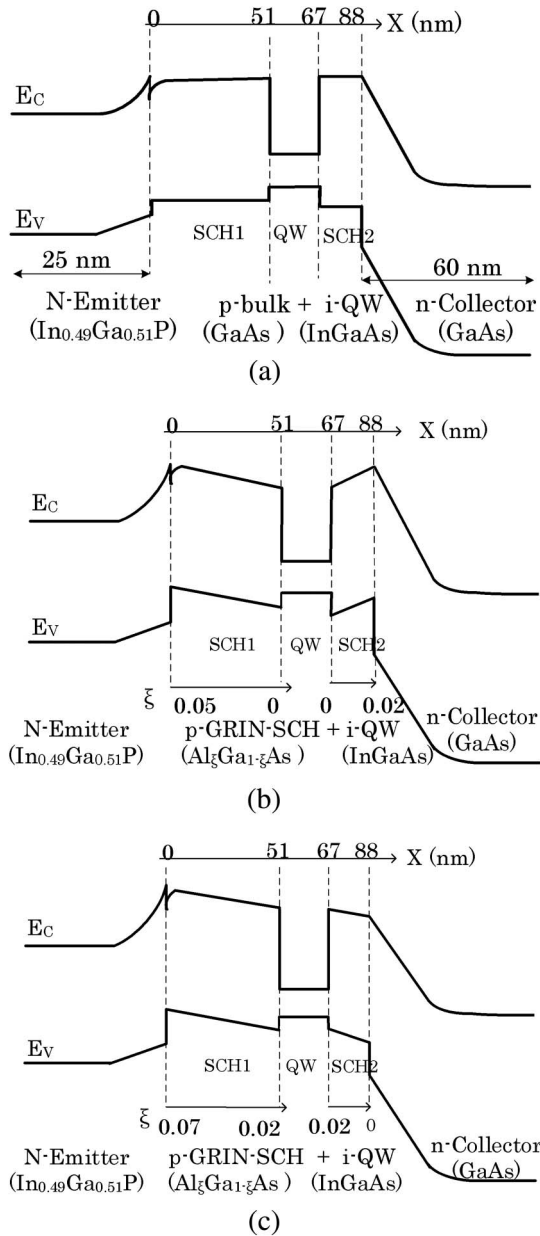


Fig. 1. Schematic energy band diagram of (a) the primary TL proposed by Feng and Holonyak^[3] (first structure), (b) first proposed GRIN-SCH structure, (second structure), and (c) second proposed GRIN-SCH structure (third structure) under forward bias. Slope of the band diagram in SCH1 and SCH2, which determines the magnitude of the quasi-electric field.

$$D_2 \frac{\partial^2 n}{\partial x^2} + \mu_2 \varepsilon_2 \frac{\partial n}{\partial x} - \frac{n}{\tau_{B2}} = 0 \quad \text{SCH2}, \quad (4)$$

where μ_1 and μ_2 are the effective minority electron mobilities, corresponding to SCH1 and SCH2, and τ_{B1} and τ_{B2} are the average recombination lifetimes related to SCH1 and SCH2, respectively. The boundary conditions needed to solve Eqs. (3) and (4) are $n(W_B) = 0$, and $n(W_{qw}^-) = n(W_{qw}^+) = N_{V,S}$, where $N_{V,S}$ is the carrier density of the virtual states (VS) located at $x = W_{qw}$.

The current density of the VS ($J_{V,S}$), including both the drift and diffusion components, is

$$J_{V,S} = \underbrace{qD_1 \frac{\partial n}{\partial x}(W_{qw}^-) - qD_2 \frac{\partial n}{\partial x}(W_{qw}^-)}_{\text{diffusion component}} + \underbrace{q\mu_1 n(W_{qw}^-)\varepsilon_{B1} - q\mu_2 n(W_{qw}^-)\varepsilon_{B2}}_{\text{drift component}}. \quad (5)$$

Finally, the emitter and collector current densities are found by

$$J_E = \underbrace{qD_1 \frac{\partial n}{\partial x}}_{\text{diffusion component}} + \underbrace{q\mu_1 n(x)\varepsilon_1}_{\text{drift component}}; \quad x = 0. \quad (6)$$

$$J_C = \underbrace{qD_2 \frac{\partial n}{\partial x}}_{\text{diffusion component}} + \underbrace{q\mu_2 n(x)\varepsilon_2}_{\text{drift component}}; \quad x = W_B. \quad (7)$$

Also, the current relation of the transistor is $j_E = j_C + j_B$.

The laser is described by the conventional laser rate equations^[6]

$$\frac{dS}{dt} = \left(\Gamma G(n_{QW}, S) - \frac{1}{\tau_P} \right) S + \Gamma R'_{sp}, \quad (8)$$

$$\frac{dn_{QW}}{dt} = \frac{j_{QW}}{qd} - \frac{n_{QW}}{\tau_S} - G(n_{QW}, S)S, \quad (9)$$

$$G(N_{QW}, S) = \frac{G_0(n_{QW} - N_{tr})}{1 + \varepsilon S}. \quad (10)$$

The QW in the base location adds another recombination region that has a variable recombination rate; spontaneous emission below the laser threshold and stimulated emission above the laser threshold. Carriers at $x = 0$ are located at the virtual bound states. The carriers entering the VSs have two possibilities, falling in the QW states or diffusing to the collector. Equations (11) and (12) make appropriate connections between carrier densities and current densities related to the QW (n_{QW} , j_{QW}) and VS^[7]:

$$\frac{j_{V,S}}{qd} = \frac{j_{QW}}{qd} - \frac{n_{V,S}}{\tau_S}, \quad (11)$$

$$\frac{j_{QW}}{qd} = \frac{n_{V,S}}{\tau_{cap}} - \frac{n_{QW}}{\tau_{esc}}. \quad (12)$$

In the above equations, S is the photon density, Γ is the optical confinement factor, $G(n_{QW}, S)$ denotes the optical gain, ε is the gain compression factor, R'_{sp} is the spontaneous emission, d is the QW width, $\tau_S = 1000$ ps is the spontaneous emission lifetime, and $\tau_{esc} = 10$ ps is the escape lifetime from the QW to the VS^[8]. τ_{cap} is the overall capture lifetime for the QW^[9].

Table 1. Calculated Physical Parameters for All Three Structures

Device Parameter	Symbol	Unit	Calculation Approach Ref.	Structure			
				1st	2nd	3rd	
Effective minority electron mobility	SCH1	μ_1	cm^2/Vs	[12]	1068	964.7	919.325
	SCH2	μ_2	cm^2/Vs		1068	1014.05	1014.05
Diffusion constant	SCH1	D_1	cm^2/s	[4]	27.61	24.88	23.71
	SCH2	D_2	cm^2/s		27.61	26.16	26.16
Quasi-electric field	SCH1	ϵ_1	V/cm	[4]	0	1.22×10^4	1.22×10^4
	SCH2	ϵ_2	V/cm		0	1.18×10^4	1.18×10^4
Effective recombination lifetime	SCH1	τ_{B1}	ps	[9]	201	220	243
	SCH2	τ_{B2}	ps		201	210	210
Optical confinement factor		Γ	%	[9]	5.82	5.65	5.51
Optical loss		α_i	cm^{-1}	[9]	20.14	19.56	19.07
Photon lifetime		τ_p	ps	[9]	2.57	2.59	2.61
Electron capture time		τ_{cap}	ps	[9]	0.90	0.56	0.57

The semiconductor optical gain function is defined as

$$G(N_{\text{QW}}, S_0) = \frac{G_0(N_{\text{QW}} - N_{\text{tr}})}{1 + \epsilon S_0}, \quad (13)$$

where N_{tr} is the transparency electron density, S_0 is the dc value of photon concentration, and G_0 is the differential gain of the active layer. Our focus in this Letter is to apparently not alter the active region (i.e., the QW), but the SCH. The QW parameters, including G_0 and ϵ , were left unchanged in our study. In our previously published Letter, considering ground, first and second excited states, strain effects, and the calculation of quasi-Fermi levels of the conduction and valence band, a nonlinear carrier-dependent gain of the TL is developed, from which we extracted the gain parameters, i.e., ϵ and G_0 , as a function of device structural factors^[10].

The threshold gain (G_{th}) for all three structures is calculated using the optical confinement factor (Γ) and optical loss (α) of each structure,

$$\Gamma G_{\text{th}} = \alpha + [1/(2L)] \ln[1/(R_1 R_2)], \quad (14)$$

where $L = 450 \mu\text{m}$ is the laser cavity length, and $R_1 = 0.32$ and $R_2 = 0.32$ are the facet reflectivity.

Around the threshold point, $N_{\text{QW}} = N_{\text{th}}$, and $S = 0$. Using Eq. (10), it can be shown that

$$G_{\text{th}} = G_0(N_{\text{th}} - N_{\text{tr}}). \quad (15)$$

From the calculated value of G_{th} , we deduce the corresponding N_{tr} , which gives the value of current density at transparency via the relation $J_{\text{tr}} = qdN_{\text{tr}}/\tau_s$.

The threshold current density is obtained using $J_{\text{th}} = J_{\text{tr}} + [qd/(\Gamma\eta a\tau_s)] \{\alpha + [1/(2L)] \ln[1/(R_1 R_2)]\}$, where a denotes the QW lattice constant, and η is the internal quantum efficiency^[11].

Minority electron mobility in highly doped $\text{Al}_\xi\text{Ga}_{1-\xi}\text{As}$ was calculated in Ref. [12], while other physical parameters of the multiple QW (MQW) TL, including the diffusion constant, carrier lifetimes, and optical confinement factor, are calculated by Taghavi *et al.*^[9]. All of the physical parameters for the new proposed structures are calculated and summarized in Table 1.

Solving Eqs. (3) and (4) for increasing the base current, the minority electron density in the base region can be calculated as shown in Fig. (2). Compared with the calculated electron distribution for the standard single QW (SQW) TL in Refs. [3,13], the excited electron population in the QW position is the maximum in the first proposed design [Fig. 2(a)]. Figure 2(a) is in good agreement with the calculated carrier population in the barrier layer for the linear GRIN-SCH QW laser discussed in Ref. [14]. Figure 2(b) also complies with the results of the graded base HBTs discussed in Ref. [4].

Considering the drift component, moreover the diffusion term, the collector current density can be achieved using Eq. (7). Figure 3 shows the variation of the dc current gain ($\beta_{\text{dc}} = I_C/I_B$) for all three structures. The dc current gain reduces significantly when second structure is employed. As shown in Fig. 2(a), the number of captured electrons in the QW position is the maximum value; as a result, the proportion of electrons captured by the collector is smaller, and, therefore, we should expect a reduction in the current gain.

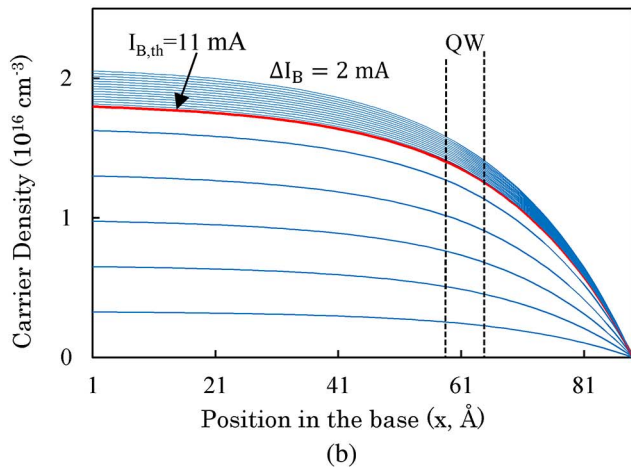
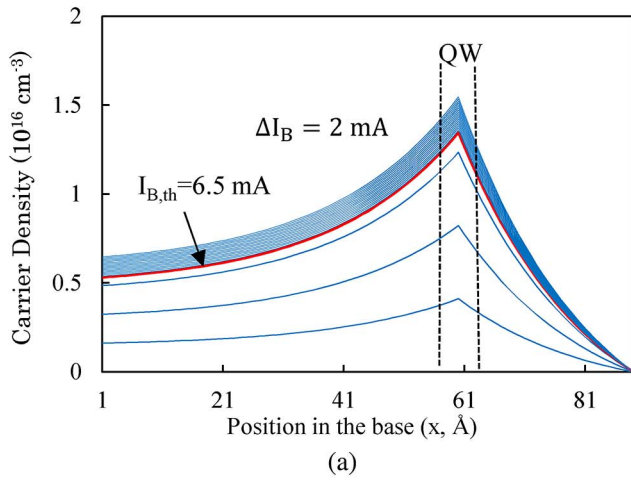


Fig. 2. Calculated minority electron distribution for (a) the first proposed GRIN-SCH structure and (b) the second proposed GRIN-SCH structure. (a) is in good agreement with the calculated carrier population for the GRIN-SCH QW laser^[14], and (b) also complies with the results of graded base HBTs^[4].

The optical output power for different base currents is calculated for the SQW TL in Ref. [11]. The optical loss and base threshold current are the main parameters affecting the output power. The calculated values of light output power for the GRIN-SCH and standard SQW TL are shown in Fig. 4. As can be seen, the optical output power for the same base current is larger for the GRIN-SCH TL compared to a standard SQW TL.

Figure 5 displays the optical frequency response of the SQW TL for different configurations (i.e., structures). One can assume that when the GRIN layers of $\text{Al}_x\text{Ga}_{1-x}\text{As}$ are utilized, the electron transport time from the emitter to the QW reduces because of the tilt in the band diagram [Fig. 1(b) and 1(c)]. Since that electron transit time is critical to the frequency response operation, the optical bandwidth increases for the GRIN-SCH structures, compared to the traditional, i.e., nongraded, structures. As reported in Ref. [15] and depicted in Fig. 5, the -3 dB optical bandwidth of the original TL (first structure) is ~ 19.5 GHz. Also, the calculated values of the

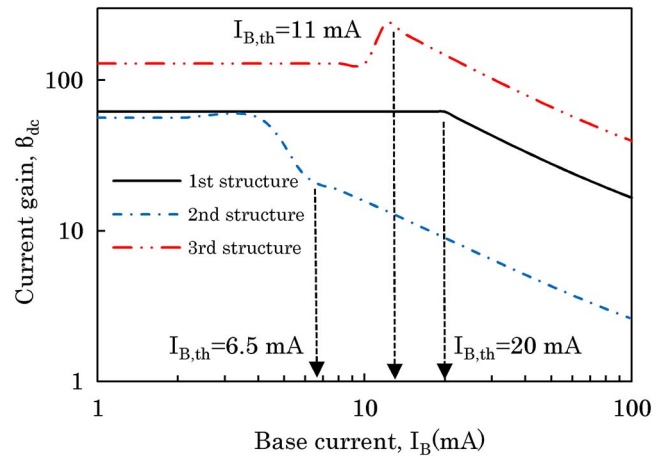


Fig. 3. Calculated dc gain $\beta_{dc}(I_C/I_B)$. The dc current gain reduces significantly, when the second structure is employed, because of the funnel form of this structure.

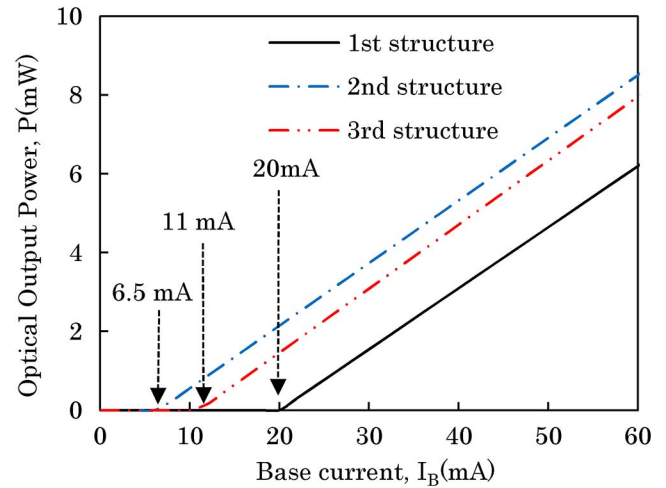


Fig. 4. Calculated optical output power P .

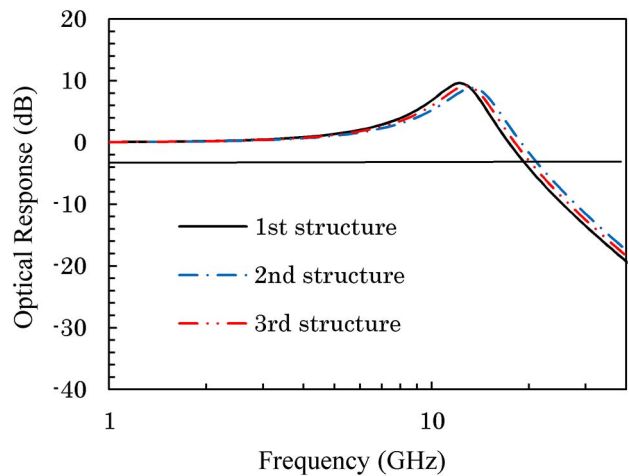


Fig. 5. Optical frequency response for the original and proposed GRIN-SCH structures. The -3 dB bandwidth of the original TL (first structure) is ~ 19.5 GHz, and for the second and third structures they are 21 and 20 GHz, respectively.

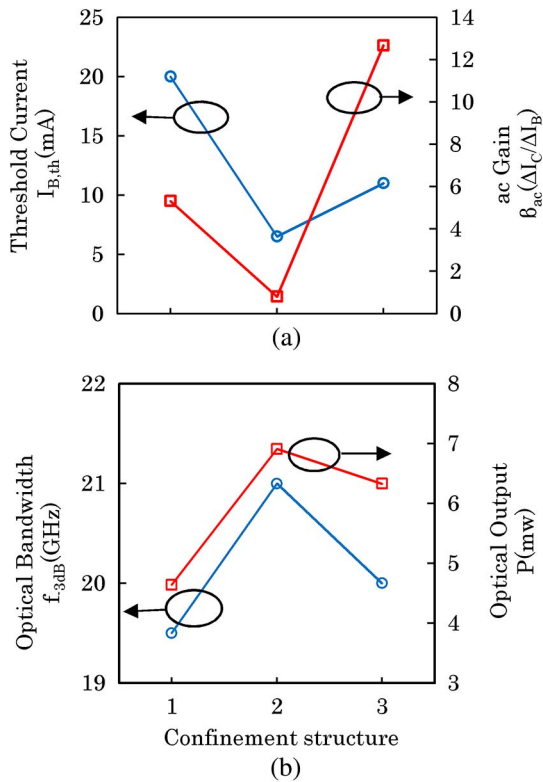


Fig. 6. Confinement structure dependency: (a) electrical and (b) optical characteristics of the SQW TL.

modulation bandwidth for the second and third structures are 21 and 20 GHz, respectively.

Figure 6 exhibits optoelectronic performances, including threshold current, ac gain, optical bandwidth, and optical power output. For optimum results in an integrated optical link or microprocessor, we need switching devices with threshold currents as low as possible, while the optical bandwidth is as high as possible. According to our simulations, structure two could be of more interest. Other characteristics, e.g. the current gain and power output, can also play important roles for specific purposes, which requires other tailored structures.

In this Letter, we theoretically study the effect of simply replacing uniform GaAs base regions with GRIN layers of $Al_\xi Ga_{1-\xi} As$. Considering the effect of the internal field due to this graded base, we develop a new continuity equation and carefully calculated all of the required physical parameters. Eventually, we show that if $Al_\xi Ga_{1-\xi} As$ ($\xi: 0.05 \rightarrow 0$ in SCH1, $\xi \rightarrow 0.02$ in SCH2) is utilized as the base region, the threshold current reduces 67% and the optical output power increases 37% compared to the previous structure with a uniform base region. Additionally, the optical bandwidth is anticipated to improve up to 21 GHz compared to 19.5 GHz in the original structure.

References

1. R. Nagarajan, M. Ishikawa, T. Fukushima, R. S. Geels, and J. E. Bowers, *IEEE J. Quantum Electron.* **28**, 1990 (1992).
2. J. Nagle, S. Hersee, M. Krakowski, T. Weil, and C. Weisbuch, *Appl. Phys. Lett.* **49**, 1325 (1986).
3. M. Feng, N. Holonyak, Jr., H. W. Then, and G. Walter, *Appl. Phys. Lett.* **91**, 053501 (2007).
4. W. Liu, *Fundamentals of III-V Devices: HBTs, MESFETs, and FETs/HEMTs* (Wiley, 1999).
5. J. H. Joe and M. Missous, *IEEE Trans. Electron Devices* **52**, 1693 (2005).
6. L. A. Coldren and S. W. Corzine, *Diode Lasers and Photonic Integrated Circuits* (Wiley Interscience, 1995).
7. B. Faraji, W. Shi, D. L. Pulfrey, and L. Chrostowski, *IEEE J. Sel. Top. Quantum Electron.* **15**, 594 (2009).
8. B. Faraji, D. L. Pulfrey, and L. Chrostowski, *Appl. Phys. Lett.* **93**, 103509-1 (2008).
9. I. Taghavi, H. Kaatuzian, and J. P. Leburton, *IEEE J. Quantum Electron.* **49**, 426 (2013).
10. I. Taghavi, H. Kaatuzian, and J. P. Leburton, *Semicond. Sci. Technol.* **28**, 025022-1 (2013).
11. R. Basu, B. Mukhopadhyay, and P. K. Basu, *Semicond. Sci. Technol.* **26**, 105014 (2011).
12. S. Herbert, *J. Appl. Phys.* **80**, 3844 (1996).
13. H. Kaatuzian and S. Taghavi, *Chin. Opt. Lett.* **7**, 435 (2009).
14. S. Morin, B. Deveaud, F. Clerot, K. Fujiwara, and K. Mitsunaga, *IEEE J. Quantum Electron.* **27**, 21 (1991).
15. M. Feng, H. W. Then, N. Holonyak, Jr., G. Walter, and A. James, *Appl. Phys. Lett.* **95**, 033509 (2009).